Probing the Chemotaxis Periplasmic Sensor Domains from *Geobacter sulfurreducens* by Combined Resonance Raman and Molecular Dynamic Approaches: NO and CO Sensing

Teresa Catarino,[†,§] Miguel Pessanha,[†] Ariel G. De Candia,[‡] Zélia Gouveia,[†] Ana P. Fernandes,[§] P. Raj Pokkuluri,[⊥] Daniel Murgida,[‡] Marcelo A. Marti,[‡] Smilja Todorovic,[*,†] and Carlos A. Salgueiro[*,§]

Instituto de Tecnologia Química e Biológica, Universidade Nova de Lisboa, Av. República (EAN), 2780-157 Oeiras, Portugal, Departamento de Química Inorgánica, Analítica y Química Física/INQUIMAE-CONICET, Facultad de Ciencias Exactas y Naturales, Universidad de Buenos Aires, Ciudad Universitaria, Pabellón 2, Buenos Aires, C1428EHA, Argentina, Requimte, CQFB, Departamento de Química da Faculdade de Ciências e Tecnologia da Universidade Nova de Lisboa, Campus Caparica, 2829-516 Caparica, Portugal, and Biosciences Division, Argonne National Laboratory, Argonne, Illinois 60439, U.S.A.

Received: April 2, 2010; Revised Manuscript Received: July 12, 2010

The periplasmic sensor domains encoded by genes *gsu0582* and *gsu0935* are part of methyl accepting chemotaxis proteins in the bacterium *Geobacter sulfurreducens* (*Gs*). The sensor domains of these proteins contain a heme-*c* prosthetic group and a PAS-like fold as revealed by their crystal structures. Biophysical studies of the two domains showed that nitric oxide (NO) binds to the heme in both the ferric and ferrous forms, whereas carbon monoxide (CO) binds only to the reduced form. In order to address these exogenous molecules as possible physiological ligands, binding studies and resonance Raman (RR) spectroscopic characterization of the respective CO and NO adducts were performed in this work. In the absence of exogenous ligands, typical RR frequencies of five-coordinated (5c) high-spin and six-coordinated (6c) low-spin species were observed in the oxidized form. In the reduced state, only frequencies corresponding to the latter were detected. In both sensors, CO binding yields 6c low-spin adducts by replacing the endogenous distal ligand. The binding of NO by the two proteins causes partial disruption of the proximal Fe-His bond, as revealed by the RR fingerprint features of 5cFe-NO and 6cNO-Fe-His species. The measured CO and NO dissociation constants of ferrous GSU0582 and GSU0935 sensors reveal that both proteins have high and similar affinity toward these molecules ($K_d \approx 0.04-0.08$ μM). On the contrary, in the ferric form, sensor GSU0582 showed a much higher affinity for NO ($K_d \approx 0.3$ μM for GSU0582 versus 17 μM for GSU0935). Molecular dynamics calculations revealed a more open heme pocket in GSU0935, which could account for the different affinities for NO. Taken together, spectroscopic data and MD calculations revealed subtle differences in the binding properties and structural features of formed CO and NO adducts, but also indicated a possibility that a (5c) high-spin/(6c) low-spin redox-linked equilibrium could drive the physiological sensing of *Gs* cells.

Introduction

Heme-based sensors are part of integrated and complex regulatory networks providing an optimized response of bacteria to changeable environments.[1−5] These proteins contain two different functional domains: the N-terminal heme domain, which acts as a sensor, and the catalytic domain. Typically, the ligand association or dissociation from the heme induces protein conformational changes that transmit signals to the catalytic domain and initiate the physiological response to the external stimulus. This process can be triggered by binding of diatomic molecules such as CO, NO, and O_2.[1,3,6,7] In Gram-positive bacteria, the heme sensor and transducer domains are both localized in the cytoplasm, while in the Gram-negative bacteria the sensor domains are located in the periplasm. The heme-based sensors described to date are all localized in the cytoplasm and contain a *b*-type heme, with exception of the chemotaxis signal transducer protein DcrA from *Desulfovibrio vulgaris*[8] and a family composed of 10 heme-based sensors, identified in *Geobacter sulfurreducens* (*Gs*).[9] The latter coded by genes *gsu0303*, *gsu1302*, *gsu2816*, *gsu2314*, *gsu0591*, *gsu0599*, *gsu0935*, *gsu0582*, *gsu2622*, and *gsu2916* contain typical signatures for *c*-type heme binding sites (CX_2CH or CX_4CH).[9] The sensor domains of proteins GSU0582 and GSU0935 (hereafter referred as 582 and 935) are part of methyl-accepting chemotaxis proteins with similar predicted topologies: an N-terminal located in the cytoplasm, followed by a transmembrane helix, a periplasmic sensor domain, another transmembrane helix, and cytoplasmic domains consisting of a HAMP domain followed by a methyl-accepting chemotaxis protein domain. The crystal structure of the periplasmic sensor domains showed that they have a PAS-like fold and form swapped dimers.[10] The swapped segment is composed of two helices at the N-terminus with the *c*-type hemes located between the two monomers. These monomers are identical in the crystals of sensor 582, whereas in the case of 935 crystals the dimer is

* Authors to whom correspondence should be addressed. (S.T.) E-mail: smilja@itqb.unl.pt. Telephone: +351 214469717. Fax: +351 214411277. (C.A.S.) E-mail: csalgueiro@dq.fct.unl.pt. Telephone: +351 2948300. Fax: +351 212948550.

† Instituto de Tecnologia Química e Biológica, Universidade Nova de Lisboa.

‡ Universidad de Buenos Aires.

§ Departamento de Química da Faculdade de Ciências e Tecnologia da Universidade Nova de Lisboa.

⊥ Argonne National Laboratory.

10.1021/jp1029882
Published on Web 08/06/2010

formed by nonidentical monomers (monomer A and B). Previous spectroscopic studies suggested that the heme groups of both proteins are high-spin ($S = 5/2$) and low-spin ($S = 0$) in the oxidized and reduced forms, respectively. Both sensor domains bind NO in their ferric and ferrous forms and CO only in the reduced form.[10] In spite of the similar structures and spectroscopic properties, the reduction potentials of the heme groups of the two sensors are quite distinct.[10]

In order to evaluate the binding properties of 582 and 935 sensor domains and if/how they discriminate between small exogenous molecules, such as NO and/or CO, we have performed affinity studies using equilibrium titrations followed by visible spectroscopy. Moreover, we took advantage of superior sensitivity and selectivity of resonance Raman (RR) spectroscopy to characterize the ligand-free and ligand-bound states of the two proteins and to probe the coordination of the hemes and their environment in the different redox states. Finally, in order to provide structural and dynamic insights that complement the observed spectroscopic results, we performed Molecular Dynamics (MD) simulations combined with hybrid Quantum Mechanics/Molecular Mechanics (QM/MM) electronic structure analysis for both 582 and 935 homodimeric proteins in the different oxidation/coordination states. The undertaken study of the oxidized and reduced forms of the two sensors in the presence and/or absence of external ligands revealed subtle differences in architecture of the respective heme pockets and their binding properties, with possible implications for signal transduction mechanism.

Experimental Methods

Cloning, Expression and Purification of Sensor Domains. The heme-containing periplasmic sensor domains 582 and 935 were produced and purified as previously described.[10] The expression and purity of the proteins were checked by SDS-PAGE using 15% polyacrilamide gels.

Determination of CO and NO Dissociation Constants. All experiments were carried out at 293 K in 20 mM phosphate buffer with 100 mM NaCl at pH 7.6. Ligand binding was monitored by UV−visible spectroscopic changes, using a Shimadzu UV-1203 spectrophotometer placed inside an anaerobic chamber, in which the oxygen level was kept below 2 ppm. All solutions and buffers were prepared inside the anaerobic chamber with degassed water. Reduced protein samples were obtained by the addition of a few microliters of a solution of sodium dithionite. Addition of excess of dithionite was avoided by checking the absorbance at 315 nm. The protein concentration in each experiment was determined from the absorbance at the γ-Soret peak (408 nm) in the oxidized form using $\varepsilon = 188\ \mathrm{mM^{-1}\ cm^{-1}}$.[11]

Analysis of the Data. Equation 1 was fitted to the experimental protein−ligand bound fraction ($Y = [\mathrm{PL}]/P_T$) as a function of total ligand to total protein concentration ratio (L_T/P_T) to obtain the dissociation constant $K_d = ([\mathrm{P}][\mathrm{L}])/[\mathrm{PL}]$. The total protein concentration corresponds to a sum of ligand-free and ligand-bound concentrations, $P_T = [\mathrm{P}] + [\mathrm{PL}]$, similarly, total concentration of ligand is $L_T = [\mathrm{L}]+[\mathrm{PL}]$, considering the equilibrium between protein P and ligand L:

$$\mathrm{PL} \rightleftarrows \mathrm{P} + \mathrm{L}$$

$$Y = \frac{\left(1 + \frac{L_T}{P_T} + \frac{K_d}{P_T}\right) - \sqrt{\left(1 + \frac{L_T}{P_T} + \frac{K_d}{P_T}\right)^2 - 4\frac{L_T}{P_T}}}{2} \quad (1)$$

In order to represent Y as a function of L_T/P_T it is necessary to express [PL] as a function of P_T, L_T, and K_d,

$$[\mathrm{PL}] = P_T - [\mathrm{P}] = P_T - \frac{K_d[\mathrm{PL}]}{[\mathrm{L}]} = P_T - \frac{K_d[\mathrm{PL}]}{L_T - [\mathrm{PL}]}$$

Rearrangement gives a quadratic equation:

$$[\mathrm{PL}]^2 - (L_T + P_T + K_d)[\mathrm{PL}] + P_T L_T = 0$$

which upon division by P_T^2 becomes:

$$\left(\frac{[\mathrm{PL}]}{P_T}\right)^2 - \left(\frac{L_T}{P_T} + 1 + \frac{K_d}{P_T}\right)\left(\frac{[\mathrm{PL}]}{P_T}\right) + \frac{L_T}{P_T} = 0$$

and can be rewritten as:

$$Y^2 - \left(1 + \frac{L_T}{P_T} + \frac{K_d}{P_T}\right)Y + \frac{L_T}{P_T} = 0$$

The solution of this equation is eq 1.

CO Binding. Degassed buffer was saturated with CO in a gas line and then transferred to the anaerobic chamber inside hungate anaerobic tubes with butyl rubber septa. The concentration of CO in these solutions is approximately 1 mM (saturation). In order to account for possible loss of CO during the experimental procedure, the exact CO concentration for each experiment was obtained from a two parameter fit of eq 1 to the data: the protein concentration was fixed and K_d and CO concentration were adjusted using the Excel tool "Solver" to give the best fit to the data. The resultant concentrations of CO in different experiments were within the 0.8 to 0.9 mM range. The titration of reduced protein with CO was performed by successive additions of several microliters of CO-saturated buffer using a gastight Hamilton syringe, followed by recording the visible spectrum. Calculation of CO-bound fraction was made by the nonlinear fit of each visible spectrum to the weighted average of reference spectra for the reduced and for the fully CO-bound forms, plus an offset constant. The spectral adjustment was made between 400 and 600 nm.[10]

Concentrations of 582 and 935 were 4.5−5.3 μM and 4−8 μM, respectively.

NO Binding. The titration of the sensors with NO was performed using a NO releasing compound, DEANONOate (Sigma Aldrich). A 32 mM stock solution of DEANONOate was prepared anaerobically in 10 mM NaOH and diluted 50 times in 10 mM NaOH before each experiment. The DEANONOate solution is stable at high pH but it starts decomposing when added to the pH 7.6 buffer. Since each mole of compound releases 1.5 mole of NO, the concentration of NO in the above solution is approximately 1 mM, after full decay of the DEANONOate. Each titration was started by the addition of 10 μL of the DEANONOate solution followed by acquisition of visible spectra at given time intervals. The NO concentration for

each spectrum was calculated from the exponential decay curve of DEANONOate, recorded on the same day, under the same experimental conditions. In most cases more than one DEANONOate addition was necessary to complete the titration. Calculation of NO-bound fraction was made by the nonlinear fit of each visible spectrum to the weighted average of a reference spectrum for the oxidized or reduced form of the sensor and a reference spectrum for the corresponding fully NO-bound form, plus an offset constant. The spectral adjustment was made between 450 and 650 nm for the reduced sensors and between 350 and 650 nm for the oxidized sensors.[10] Concentrations of 582 and 935 were 4−7.5 μM and 2−6 μM, respectively.

Raman Spectroscopy. All RR measurements were performed with a confocal microscope coupled to a Raman spectrometer (Jobin Yvon U1000) equipped with 1200 L/mm grating and liquid-nitrogen-cooled back-illuminated CCD detector. Samples were placed in a quartz rotating cell and excited with the 413 nm line from a krypton ion laser (Coherent Innova 302). Protein samples, with concentrations ranging from 40−200 μM in 20 mM phosphate buffer (pH 7.6) containing 0.1 M NaCl, were used. Oxidized (as purified) and sodium dithionite reduced samples, in the presence or absence of CO and NO, were measured with a laser power of 0.4−9 mW and accumulation times of 60 s at room temperature. The samples of fully reduced sensor domains in the presence and absence of CO and NO were prepared in the anaerobic chamber, as described above.

After polynomial background subtraction, the positions and line-widths of the Raman bands were determined by component analysis in which the spectra of the individual species were fitted to the measured spectra, performed by homemade software.

Computational Methods

Setup of the System. The initial structures of homodimeric 582 and 935 proteins were obtained from the experimental X-ray structures.[10] Starting from these initial structures the following homodimeric states were built for each protein, by adding the corresponding exogenous (CO/NO) or endogenous ligands (Met60) *in silico*: a six coordinated (6c) Histidine-Methionine state (6cHis−Met); a 6c CO-bound state (6cCO); a 6c NO-bound state of ferric heme (6cFe^{3+}NO); a 6c NO-bound state of the ferrous heme (6cFe^{2+}NO); a 5c NO-bound state of ferrous heme (i.e., where the Fe proximal His bond is broken) (5cFe^{2+}NO) and, finally a five coordinated (5c) state with only the endogenous proximal His as axial ligand (i.e., with the Fe−Met bond absent) (5cHis). It should be noted that, although this is formally a 5c state, the presence of transient water molecules electrostatically interacting with the iron is consistent with the X-ray structure showing a water molecule in place of Met60.

System Setup and Equilibration. To set up the systems for the MD simulations, the starting structures were immersed in a preequilibrated octahedral box of TIP3P water molecules. The standard protonation state at physiological pH was assigned to the ionizable residues. All simulations were performed at 1 atm and 300 K, maintained with the Berendsen barostat and thermostat, using periodic boundary conditions and Ewald sums (grid spacing of 1 Å) for treating long-range electrostatic interactions with a 10 Å cutoff for computing direct interactions. The SHAKE algorithm was used to keep bonds involving H atoms at their equilibrium length, allowing employment of a 2 fs time step for the integration of Newton's equations, using the Amber default simulation parameters. The Amber f99SB force field parameters were used for all residues.[12] The heme parameters in all coordination states used in this work were developed and thoroughly tested by our group in previous works.[13−16] Equilibration protocols consisted of performing an optimization of the initial structures, followed by a slow heating up to the desired temperature. The equilibration is performed in two steps: (i) a 500 ps constant volume MD run heats the system slowly to 300 K; (ii) another 500 ps MD run at constant pressure achieves proper density. Once the system is equilibrated, the different production MD runs are performed. Frames were collected at 1 ps intervals, which were subsequently used to analyze the trajectories.

QM/MM Calculations. QM/MM calculations were performed for the NO- and CO-bound forms of each monomer. The initial structures for the QM/MM calculations were obtained from the MD simulations. Selected snapshots for each structure were chosen and cooled down slowly to 0 K. Starting from these frozen structures full hybrid QM/MM geometry optimizations were performed by means of a conjugate gradient algorithm with the density functional theory (DFT) approximation programmed within the SIESTA code using our own QM/MM implementation basis sets and parameters, which has proven to be successful for the study of biological systems, especially heme proteins. Further technical details about the QM/MM implementation can be found elsewhere.[13,16,17] Both the MD and QM/MM schemes and protocols presented here have been widely used and thoroughly tested for several heme proteins in previous works.[13,16,17]

Results and Discussion

Ligand-Free 582 and 935. The RR spectra of heme proteins, obtained upon excitation under Soret band, provide information on redox, spin, and coordination state of the heme group, based on frequencies of core-size marker bands that are found in the high-frequency region. The spectra of the oxidized forms of sensors 582 and 935 (Figure 1A) reveal substantial heterogeneity. The characteristic frequencies of ν_3, ν_2, and ν_{10} bands, determined accurately by component analysis, reveal the presence of at least two spin populations in both proteins. Vibrational modes ν_3 and ν_2 found in the spectra of 582 at 1483 cm^{-1} and 1567 cm^{-1}, respectively (1479 cm^{-1} and 1570 cm^{-1} for sensor 935), are typical for 6cHS *c*-type hemes, while those at 1508 cm^{-1} (ν_3), 1588 cm^{-1} (ν_2), and 1642 cm^{-1} (ν_{10}) are characteristic for 6cLS ferric hemes (Table 1).[18] The low-spin (LS) population is more abundant than the high-spin (HS) in the 935, as it is clear from the relative ratio of the HS (1479 cm^{-1}) to LS (1508 cm^{-1}) ν_3 mode intensities (Figure 1A, lower trace). In the case of the sensor 582 the HS and LS bands appear with almost 1:1 intensity (Figure 1A, upper trace). However, since the HS species has a higher molar intensity, we conclude that the LS species is also predominant in this sensor. The relative HS:LS intensity ratio of the two spin state marker bands, ν_3 and ν_2, indicates that a higher amount of 6cHS species is present in 582 than in 935 sensor (Figure 1A). Two spin states were identified earlier from the EPR spectra of these proteins at low temperatures, but could not be discriminated by NMR or UV−visible spectroscopy.[10] The crystal structure of the ferric sensors reveals the existence of both HS (His−Fe−H_2O) and LS (His−Fe−Met) species in 935, while the crystals of 582 possess only the former ligation. Coexistence of two species is apparent in RR spectra regardless of the protein concentration (40−200 μM) or laser power (0.4−9 mW), thus being an intrinsic property of the sensors at room temperature and neutral pH. RR spectra of DevS642 sensor also reveal a coexistence of two spin states, with the ν_4, ν_3, ν_2, and ν_{10} modes at frequencies

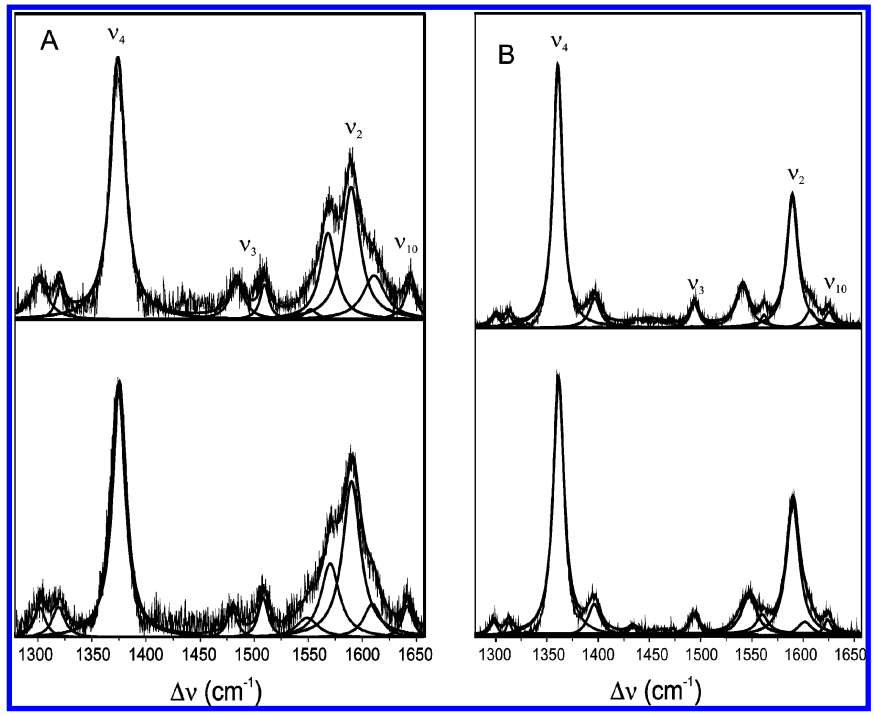

Figure 1. Experimental and component RR spectra in the high-frequency region of oxidized (A) and reduced (B) forms of the 582 (top) and 935 (bottom) sensors. Experimental conditions: excitation 413 nm, accumulation time 60 s, laser power (A) 2 mW and (B) 4 mW, concentration of the proteins (A) 40 μM and (B) 200 μM.

TABLE 1: Summary of the RR Vibrational Modes of 582 and 935 Sensors[a]

	ν_4 (cm^{-1})	ν_3 (cm^{-1})	ν_2 (cm^{-1})	ν_{10} (cm^{-1})	$\nu/\delta_{Fe\text{-}CO}$ (cm^{-1})	spin state
Fe^{3+}−935	1374	1479/1508	1570/1590	1641		6cHS/6cLS
Fe^{2+}−935	1361	1494	1590	1624		6cLS
Fe^{2+}−CO−935	1371	1497	1591	1631	494/566	6cLS
Fe^{3+}−NO−935	1373/1379	1503/1512	1592	1644		6cLS/5cHS
Fe^{2+}−NO−935	1372/1379	1503/1510	1593	1636/1645		6cLS/5cHS
Fe^{3+}−582	1373	1483/1508	1567/1588	1642		6cHS/6cLS
Fe^{2+}−582	1360	1494	1589	1625		6cLS
Fe^{2+}−CO−582	1371	1497	1590	1632	482/567	6cLS
Fe^{3+}−NO−582	1374/1380	1501/1510	1591	1644		6cLS/5cHS
Fe^{2+}−NO−582	1374/1380	1503/1512	1591	1637/1645		6cLS/5cHS

[a] Oxidation (ν_4) and spin/coordination state (ν_3, ν_2, and ν_{10}) marker bands are indicated, together with Fe-CO stretching (ν) and bending (δ) modes, obtained by component analysis of the RR spectra.

almost identical to the ones observed in the spectra of 582 and 935, for both HS and LS populations under the same experimental conditions.[19] The physiological reason for the existence of equilibrium of the spin states is not clear. However, a 'dynamic' nature of the ferric heme pocket is apparent and corroborated by a change of the coordination state upon reduction (see below).

RR spectra of sodium-dithionite reduced 582 and 935 reveal much higher homogeneity, being dominated by spin state marker bands characteristic of 6cLS (Figure 1B and Table 1). As postulated earlier,[10] the weak sixth ligand (H_2O) has to be replaced by an endogenous ligand upon reduction in order to give 6cLS species. The distal axial ligand in the crystal structure of monomer B of 935 sensor, Met60, was identified as the most likely candidate for the sixth ligand in ferrous sensors.[10]

CO Binding. Sensors 582 and 935 bind CO only in the reduced form.[10] The UV−visible spectra undergo significant changes upon addition of CO (Figure 2) and therefore were used to determine the binding (or dissociation) constants of CO to the ferrous sensors. For each sensor the fraction bound to the ligand was calculated as described in the Experimental Methods.

The CO titration of sensor 582 and the respective binding curve are shown in Figure 2. It is apparent from the values in

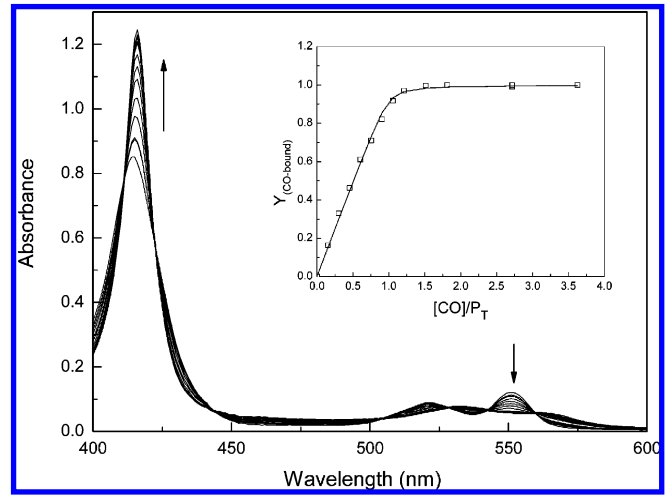

Figure 2. Titration of reduced sensor 582 with CO. Electronic absorption spectral changes after addition of CO. The arrows indicate the sequence of data collection. The inset shows the variation of the CO-bound fraction versus the ratio [CO]/P_T. The solid line was generated using eq 1 and the dissociation constant listed in Table 2.

TABLE 2: Dissociation Constants (μM) for Sensor Domains 582, 935, and DcrA[8]

sensor	$Fe^{2+}-CO$	$Fe^{2+}-NO$	$Fe^{3+}-NO$
582	0.05 ± 0.03	0.08 ± 0.01	0.34 ± 0.1
935	0.08 ± 0.04	0.04 ± 0.02	17 ± 3
DcrA	138	–	–

Table 2 that the ferrous 582 and 935 bind CO with very high affinity and, moreover, that the CO dissociation constants (0.05 μM and 0.08 μM for 582 and 935, respectively) do not indicate discrimination between the two sensors. Besides the sensors 582 and 935, the chemotaxis signal transduction protein DcrA from bacterium *Desulfovibrio vulgaris* is the only reported periplasmic sensor with *c*-type heme which also binds CO in the reduced form.[8] With the exception of the residues that bind to the heme group, DcrA sensor shares only 30% and 21% sequence identity with 935 and 582, respectively. Despite the moderate amino acid sequence identity between the DcrA and the two *Gs* sensors, they display remarkable similarities in visible and RR spectral properties in CO bound state (see below). However, the affinity of 582 and 935 sensors for CO is several orders of magnitude higher than that of DcrA (see Table 2).[8] This discrepancy can be attributed to the putative role of sensor DcrA, associated with sensing O_2 and/or redox potential.[8]

The RR spectra of carbonyl adducts of 582 and 935 ferrous sensors show an upshift of the ν_4 mode, which is found at 1371 cm^{-1}, at the position characteristic for ferric hemes (Figure 3, right panel, ferrous 582 CO adduct). This shift is a consequence of a significantly altered electronic distribution at the ferrous iron in the $Fe^{2+}-CO$ adduct, in comparison with Fe^{2+}, caused by electron withdrawal from the iron ion (but not its oxidation) as judged from the frequency of the electron density indicator, ν_4. All studied samples were, after RR measurements, carefully transferred into a cuvette for UV−visible spectroscopy and measured in an anaerobic environment. The UV−visible spectra confirmed that the RR spectra originated from the $Fe^{2+}-CO$ adduct. The frequency of the spin/oxidation state marker band ν_3 also unambiguously points to the ferrous iron (Table 1). Similarly, a large upshift of ν_4 mode was observed in CO complexes of ferrous guanylate cyclase (sGC) and CO-sensing transcriptional activator (CooA), and attributed to a π back bonding from Fe^{2+} to the CO ligand.[20−23] Carbonyl adducts of ferrous cytochrome *c*' and sGC both show ν_4, but also ν_{10}, at relatively high frequencies, as observed here for 582 and 935 proteins.[21,23,24] The Fe^{2+}-CO adducts of 582 and 935 sensors are clearly in 6cLS state, as indicated by the frequencies of ν_3 and ν_2 modes (Table 1). This finding further supports the axial ligand exchange upon CO binding to the LS ferrous sensors (i.e., CO displacing the endogenous distal ligand of the heme), as it is the case of many other heme sensor proteins.[10,19−25]

In the low-frequency region, RR spectra contain Fe-axial ligand stretching and bending modes, allowing identification of the ligand and characterization of its environment. In the low frequency region of RR spectra of 582 and 935 sensors, two additional bands appear in the presence of CO (Figure 3, left panel, traces a and b, respectively). They originate from the Fe−CO stretching and bending modes, which are clearly absent from the spectra of the CO-free 582 and 935 (Figure 3, left panel). The more intense modes, attributed to Fe−CO stretching coordinates, fall into 473−512 cm^{-1} range as it is also the case for various *c*-type heme−CO adducts.[21,23,24] The energy of the Fe−CO stretching is significantly downshifted in the 582 protein (482 cm^{-1}) in comparison with 935 (494 cm^{-1}), implying a weaker Fe−CO bond in the former sensor.

582 and 935 NO Adducts. Similarly to the experiments with CO, NO binding to 582 and 935 sensors was followed spectrophotometrically. Unlike CO which binds only to the reduced form of the sensors, NO binds to both ferric and ferrous hemes (Table 2). The determined equilibrium dissociation constants show that NO binds to the ferrous sensors with a higher affinity. This difference is more pronounced in the 935 sensor, for which the affinity of the ferric form is 3 orders of magnitude lower (Figure 4). Moreover, the affinity of each reduced sensor for CO is of the same order of magnitude as its affinity for NO.

The RR spectra of the $Fe^{2+}-NO$ adducts reveal the presence of two spin populations (Figure 5A). Indeed, a careful band fitting analysis shows that in order to reproduce the ν_4, ν_3, ν_2, and ν_{10} modes in the NO adduct spectra, two well-separated bands of line-widths consistent with respective natural line-widths (for instance 14−15 cm^{-1} for ν_4 and 8−10 cm^{-1} for ν_3 mode) are required for each mode. Both spin species in both proteins show up-shifted frequencies of the marker bands for a ferrous state (Table 1). One spin state, with ν_4, ν_3, and ν_{10} at 1379, 1510, and 1645 cm^{-1} (for 935), has a RR fingerprint very similar to that of NO adducts of ferrous CooA, sGC, and cytochrome *c* ′, attributed to the ferrous 5cHS−NO state with no proximal ligand.[21−24,26] Nitric oxide is well-known as a strong

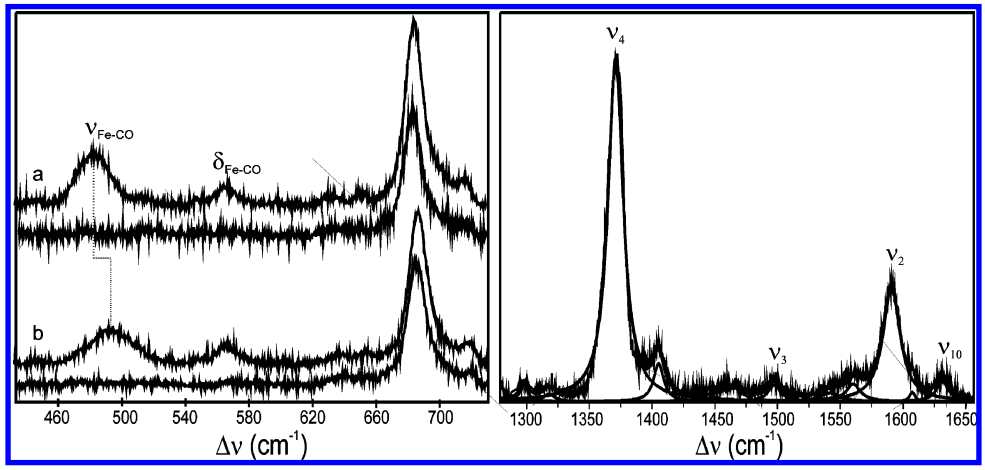

Figure 3. CO binding to ferrous forms of the sensors 582 and 935. (Left panel) Low-frequency RR spectra of (a) 582 in the absence (lower trace), and in the presence (upper trace) of CO; and (b) 935 in the absence (lower trace) and in the presence (upper trace) of CO. (Right panel) High-frequency RR spectra (experimental and component) of 582 in the presence of CO. Experimental conditions as in Figure 1.

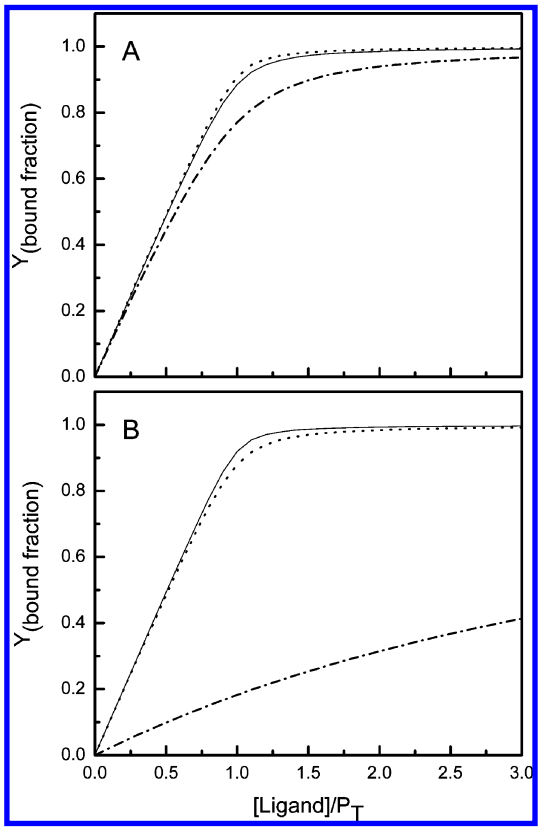

Figure 4. Simulated bound fraction curves for sensors 582 (A) and 935 (B). The curves were calculated using eq 1 and the K_d values listed in Table 2: Fe^{2+}−CO (dotted), Fe^{2+}−NO (solid), and Fe^{3+}−NO (dashed−dotted).

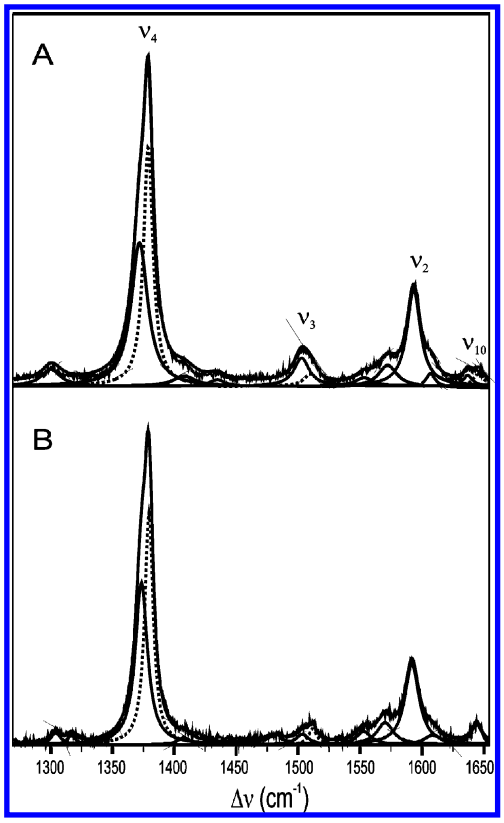

Figure 5. Binding of NO to 935. High-frequency region RR spectra (experimental and component) of (A) ferrous and (B) ferric 935−NO adduct. Solid line: 6cLS, dotted line 5cHS state. Experimental conditions as in Figure 1, except for the protein concentration (200 μM in both cases).

trans labilizing ligand in its heme complexes, which can lead to disruption of the bond between the heme iron and proximal His ligand, resulting in 5cHS Fe^{2+}−NO complex. This species possesses atypically high frequencies for ν_4, ν_3, ν_2, and ν_{10} bands as demonstrated for model compounds and various NO binding heme proteins.[19,21−24,26,27] The second species, with ν_4, ν_3 and ν_{10} at 1372, 1503, and 1636 cm^{-1} (for 935) attributed to 6cLS population, most likely originates from His−Fe^{2+}−NO adduct.[22] It has a decreased electron density at the ferrous iron, revealed by an upshift of marker band frequencies. The 6cLS species is relatively more abundant in 935, as demonstrated by the ratio of the intensities of ν_3 modes (1503 cm^{-1} for 6cLS and 1510 cm^{-1} for 5cHS) in the respective spectra of the two proteins (Figure 5A for 935, data for 582 not shown). Special care was taken in order to verify the redox state of the sensors after RR measurements (vide supra), which remained in the Fe^{2+}−NO bound form, as concluded from the UV−visible spectra of respective NO adducts.

As observed here for 582 and 935 sensors, NO adducts of prokaryotic homologues of sGC: L1 H-NOX domain, L2 H-NOX both from *Legionella pneumophila* and *Np* H-NOX from *Nostoc punctiforme*, are also mixtures of 5cHS and 6cLS states at physiological temperatures. These species show temperature-dependent reversible equilibrium with the 6cLS state (His-Fe^{2+}−NO) more populated at lower temperature. The latter species shows fingerprint frequencies of 6cLS state with ν_4, ν_3 ν_2, and ν_{10} at 1372, 1500, 1586, and 1633 cm^{-1}, respectively,[25] identical to those observed for 582 and 935 sensors. Other heme sensors, such as CooA and sGC react with NO, forming exclusively five coordinated adducts in the ferrous form.[21−24]

Two spin populations were also detected in the RR spectra of 582 and 935 upon binding of NO to the ferric proteins (Figure 5B, ferric 935−NO adduct), as revealed by the component analysis of the spectra (Table 1). The features of one spin population, with up-shifted ν_4, ν_3, and ν_{10} frequencies at 1379, 1512, and 1644 cm^{-1}, respectively, remarkably resemble the RR features of 5cHS Fe^{2+}−NO adducts. Given the high solvent exposure of the heme pocket (see below) it is not unlikely that these modes originate from 5cHS Fe^{2+}−NO adducts formed by reductive nitrosylation, which is a common reaction of NO with ferric hemes.[28] Similarly, Fe^{3+}CooA−NO adduct forms the same 5cHS species, as indicated by the RR spectra, observed in the reaction of Fe^{2+}CooA with NO.[22] The second species identified in ferric NO-sensor samples (ν_4 and ν_3 at 1373 and 1503 cm^{-1}) is clearly a 6cLS ferric heme, attributed to the expected Fe^{3+}−NO adduct.

MD Simulations of 582 and 935 Sensors. In order to provide a structural and dynamic insight into the observed spectroscopic results we have performed 25 ns long MD simulations combined with QM/MM optimizations (of selected snapshots) for both 582 and 935 homodimeric sensors in different oxidation and coordination states. All studied states were stable during the simulation as evidenced by the average monomer Cα-rmsd values with respect to the X-ray structure, which are below 2.0 Å for all cases. To compare the structural and dynamic behavior of each state, the 5cHis state, which is present in three out of four hemes in the starting structures, was used as the reference state. We observe that in 582 5cHis state, the distal heme cavity remains considerably open. This leads to entering of water molecules that interact with the iron, explaining the crystal structure[10] and 6cHS His−Fe−H_2O state observed by RR. The main relevant atoms that line the distal cavity are the Met60 sulfur (Met60S) and Met60 carbonyl oxygen (Met60CO). Along the dynamics the Fe−Met60S and Fe−Met60CO distances are

TABLE 3: Average Structure RMSD Using the 5cHis and 6cHis−Met States As a Reference[a]

	reference state			
	582 5cHis	582 6cHis−Met	935 5cHis	935 6cHis−Met
6cHis-Met	2.27	0	1.54	0
6cCO	2.35	1.62	1.25	1.13
$6cFe^{3+}$−NO	2.26	1.61	1.25	0.91
$6cFe^{2+}$−NO	2.5	1.92	1.28	2.12
$5cFe^{2+}$−NO	2.2	1.62	2.02	1.11

[a] All RMSD units are Å.

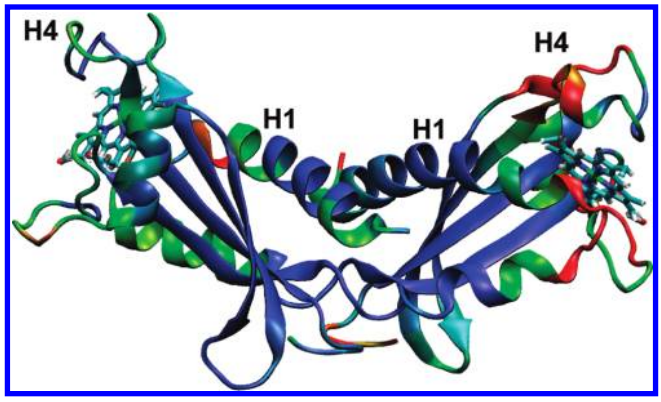

Figure 6. Structural differences between 582 5cHis and 582 6cHis−Met averaged structures. Color code is the following: blue: no change; green: 2−4 medium change; red: maximum change.

5.95 ± 0.8 Å and 4.3 ± 0.6 Å respectively (average for both subunits) and no significant difference is observed between the subunits. The Fe−Fe distance remains close to that found in the X-ray structure of 582 (49.6 ± 0.9 Å). In 935 5cHis state, the distal heme cavity also remains open and the equivalent residues Met60S and Met60CO line the distal pocket with average distances to iron of 6.25 ± 0.6 Å and 4.28 ± 0.6 Å, respectively. The Fe−Fe distance is shorter than in 582, but it is slightly larger (45.9 ± 0.9 Å) than that observed in the crystal structure (41.5 Å). The open distal cavity is consistent with the ability of both proteins to bind exogenous ligands.

In order to gain further insight into the possible structural differences between different spin/coordination states for each protein, we determined backbone rmsd for all states using both the 5cHis and 6cHis−Met structures as references (Table 3). As shown in the Figure 6 for sensor 582, the main changes between the structures are located in the heme boundaries: (i) at the proximal heme side, moving of the helix (H4) and its connecting loops; and (ii) at the heme distal side, formed by the C-terminal of helix H1 and H1−H2 loop, and the N-terminal part of H2. The domain S1−S4 beta strand core remains rigid and retains a very similar structure in all studied states. Although smaller, the structural differences in 935 are similar to those found for 582. Location of the differences, however, coincides with those found for 582 protein. Dynamical fluctuation pattern is very similar in all studied states, for both proteins.

CO Binding. In the next step, we analyzed specifically the $6cFe^{2+}$−CO ligand-bound structures and dynamics, and the respective electronic structures as determined by QM/MM calculations (summarized in Table 4). The results (Table 3) indicate that for 582 all ligand-bound states are more similar to the 6cHis−Met state (all rmsd values are below 2), than to the 5cHis state (all rmsd values above 2). Considering the average rmsd values with respect to the original structure, it is clear that at least during the simulation time, structures of all states remain very similar, and only minor changes are observed.

TABLE 4: Summary of QM/MM Calculations

	6cCO		$6cFe^{3+}$NO		$6cFe^{2+}$NO	
protein	582	935	582	935	582	935
Fe−X (Å)	1.76	1.77	1.65	1.66	1.75	1.75
X−O (Å)	1.18	1.18	1.16	1.16	1.20	1.21
Fe−X−O (deg)	177	178	173	174	140	138
Fe−His (Å)	2.09	2.06	2.05	2.01	2.21	2.21
qXO (*e*)	−0.018	0.002	0.286	0.294	−0.027	−0.121
qHis (*e*)	0.190	0.202	0.304	0.284	0.153	0.117
qFe (*e*)	0.674	0.674	0.650	0.644	0.670	0.676
$XO-S_{Met60}$ (Å)	5.06	5.17	3.77	3.49	3.74	5.25
$XO-CO_{Met60}$ (Å)	2.98	3.58	2.88	2.95	3.45	4.76

In 582 protein, the distal cavity where the CO ligand is placed is lined by H1−L2 loop. Specifically, residues Met60, Met61, Ala62, Gly63, Asp64, and Met65, and the side chains of Met60 and Met65 look toward the ligand (Figure 7A), side-chains of residues 61 to 63 point into the solvent, leaving their backbone lining the ligand-bound position. Also, Val67 and Ile68 close the distal heme pocket from above. Specific distal ligand−protein interactions are scarce; the Met60S remains at about 5 Å from the ligand, while Met65SCH_3 group faces the ligand on the other side. The possible strong electrostatic interactions may come from Met60CO and Ala62NH groups, which are at average distances of 2.98 and 3.44 Å from the ligand. They are however involved in establishing a strong and stable hydrogen bond between themselves as a result of the H1−H2 turn. In 935, the heme distal site is also formed by the H1−H2 of the other subunit, with residues Met60, Met61, Lys62, Gly63, and Asp64. The higher polarity of Lys62 compared to Ala62 in 582 and the lack of Met65 (Ser in 935) makes the resulting distal pocket more open on the H2 side, which results in the presence of several water molecules close to the ligand (Figure 7B). In 935, Met60S is slightly closer to the ligand compared with 582 (about 4.3 Å), while Met60CO and Lys62NH are at similar average distances. Also, a strong and stable hydrogen bond is established between Met60CO and Lys62NH as a result of the H1−H2 turn.

Taken together MD and QM/MM data point to some subtle differences between the heme pockets of the two sensors that can help us understand slightly stronger Fe−C(O) bond in 935, revealed by the RR spectra. Namely, in 582 the Met60CO is closer to the ligand (Table 4) and this negative polarity of the pocket possibly affects the Fe−C(O) and CO stretching. In addition, along the MD data, sensor 935 has a more open, and therefore solvated pocket. Positive distal polar interactions tend to increase the Fe−C(O) stretching frequency and decrease the intensity of the RR $\nu_{Fe-C(O)}$ band, the latter being attributed to a reduction in Fe−C(O) bond displacement between the ground and excited state,[29] while the opposite is expected for a negative environment, as observed for 582.

NO Binding. Spectroscopic data of 582−NO and 935−NO adducts were further evaluated by the MD and QM/MM calculations (Table 4). In the $6cFe^{2+}$−NO state the ligand is almost neutral and bent, it rotates freely around the Fe−N bond, and no specific ligand distal interactions are established. For this complex, however, more interesting is the proximal site, since the $6cFe^{2+}$−NO complex is in equilibrium with the $5cFe^{2+}$−NO complex due to breaking of the Fe−His bond, as shown by RR spectra. Inspection of the proximal site of 582 shows that proximal His is well solvated, forming only temporary hydrogen bond with water molecules through the ring proton H_δ. The presence of a neutral histidine (as confirmed by the QM/MM data in Table 4), similar to the one found in FixL protein or the hemoglobin alpha chain,[30] is consistent with the lability of the Fe−His bond that yields the 5cNO state. The

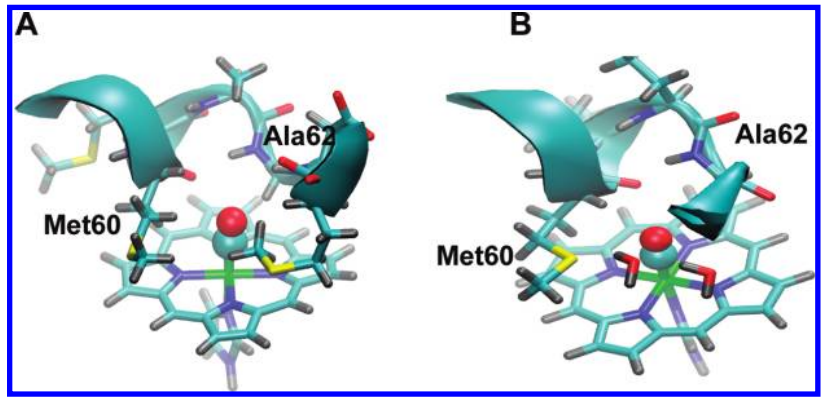

Figure 7. CO bound distal cavity of 582 (A) and 935 (B) sensors.

NO trans effect is also clearly evidenced by the QM/MM data showing an increase in the Fe−His bond in the Fe^{2+}−NO state.[30,31] Interestingly, parallel to the His ring is the side chain of Asn151 with the amide dipole aligned with His ring dipole. In 935 where the Asn151 is replaced by Leu residue, NO also freely rotates in the distal site, and no specific interactions are present.

Moreover, breaking the Fe−N(His) bond to yield the 5cFe^{2+}−NO state does not produce significant changes in either of the proteins, the proximal His remains close to the iron (N_ε−Fe distance around 3.0 Å) and only temporarily forms a weak hydrogen bond with Asn151−NH_2 in 582. In 935 Asn is replaced by Leu151, and no hydrogen bond is established. This finding can be rationalized in terms of the Cys143−His144 bond, with the first residue being covalently bound to the heme, which retains the His144 in its proximity. Furthermore, a tight hydrogen bond is present between proximal His (His144) backbone NH and the carbonyl group of the second heme covalently bound cysteine (Cys140), that impedes His backbone rotation. The only possible movement for His144 is rotation around the C_β−C_γ bond that moves the N_ε further away from the iron (to about 4.5 Å). This rotation is observed and maintained along the whole simulation for one of the 935 subunits. The observation that, upon breaking of the proximal Fe−His bond, the His remains close to the iron is consistent with the spectroscopic data showing that NO binding to ferrous iron produces a mixture of 6cFe^{2+}−NO and 5cFe^{2+}−NO species. This also corroborates the absence of new interactions involving the His residue in the 5c state upon breaking of the Fe−His bond.

The calculations also provide further insights into the binding data, that revealed much higher K_d(NO) for the ferric 935 than those measured for the 582, as shown in Table 2. This finding can be rationalized in terms of distal pocket accessibility, which was shown to be determinant for the mechanism of NO release from ferric hemes in NO carrier proteins, nitrophorins.[32,33] Namely, although the MD simulations of the ligand bound species indicate that no significant distal interactions are present in either of the proteins, it is clear from the comparison of the two distal cavities that 935 heme pocket is far more open than that in 582. This could account for a higher dissociation rate for NO in the Fe^{3+}−NO complex. Fe^{3+}−NO complexes are labile, and thermal breaking of the Fe−N bond occurs fast. An increased solvent accessibility in the heme cavity of 935 therefore favors NO displacement by the incoming water molecules. The closed heme pocket of the 582 sensor, on the other hand, will retain the free NO more efficiently, which would result in a lower dissociation rate. The 5cHS−NO bound population is, consequently, more abundant in the RR spectra of the ferrous 582−NO adduct, as judged by the relative intensity ratio of the ν_3 modes at 1503 (6cLS) and 1512 cm^{-1} (5cHS) (data not shown).

Moreover, along the dynamics the 582 Fe^{3+}−NO structure is very similar to the CO bound state, as it is expected, since Fe^{2+}−CO and Fe^{3+}−NO are isoelectronic and display the same Fe−X−O angle of around 180°. The main difference is the charge on the ligand, as shown by the QM/MM calculations: while CO is close to neutral and can be even slightly positive, the NO in the Fe^{3+}−NO state has significant positive character, showing a clear $(Fe^{2+}-NO)^+$ state behavior. As a result, a shorter NO−Met60CO distance is observed (average distance of 2.88 Å) and also a shorter NO−Met60S distance (average of 3.35 Å) compared to the CO bound state. Consistently, the NO−Ala62NH is larger. The same trend is observed for 935 Fe^{3+}−NO dynamics (Table 4).

Conclusions

Despite a moderate sequence homology, the 582 and 935 sensors reveal remarkably similar spectroscopic features, as previously shown by UV−visible, EPR, and NMR data.[10] The fundamental question in addressing the physiological role of 582 and 935 sensors is the identification of the signal that they sense, and how the signal is transduced. In order to discriminate between sensing of CO and NO as possible physiological signals, we studied the structural and dynamic effects produced by these ligands on the PAS-like domain of the two proteins. The superior sensitivity of RR spectroscopy toward the spin/coordination state of the heme group coupled to the quantitative determination of the dissociation constants was used to distinguish between the binding of NO and CO. In order to investigate possible physiological on/off states, the spectroscopic results were further rationalized by MD and QM/MM calculations by comparing the different protein states, structurally and dynamically. Taken together the RR, MD, and binding studies revealed several common features for both sensors: (i) presence of two spin populations (HS and LS) in the ferric state; (ii) conversion into LS population upon reduction; (iii) CO binding to the ferrous proteins forming 6cLS−CO species by replacing the distal endogenous axial ligand; (iv) NO binding to both ferric and ferrous proteins, and formation of 5cHS−NO and 6cLS−NO species in both redox states.

In addition, in the ferrous form, the periplasmic sensors 582 and 935 do not show any discrimination between the two diatomic gases. In the ferric form, however, the 582 reveals much higher affinity for NO. This finding correlates well with the more open distal heme cavity observed in 935. Typically, the affinity of heme proteins toward NO is orders of magnitude

higher than that for CO,[34−39] and in that respect, the 935 and 582 are unusual. The dissociation constants determined in this work, however, fall within the range of those reported for other CO and NO adducts of ferrous heme proteins, being at the lower limit for the former and at the upper limit for the latter in the case of the GSUs.

The results from the present work show that both CO and NO bind in a similar manner to the distal face of the ferrous heme by replacing the endogenous Met60 ligand. However, due to the intrinsic properties of each ligand, significantly different effects occur upon binding. The formation of 5cFe−NO complexes clearly demonstrates that the NO trans labilizing effect is operational in both ferrous sensors. It weakens the proximal His−Fe bond, which is about 2.21 Å in these complexes compared to about 2.05 Å in the Fe^{2+}−CO or Fe^{3+}−NO states as observed in MD simulations. In 582 and 935 sensors NO only partially breaks the proximal His−Fe bond. This finding can be rationalized by the fact that the proximal His is part of the heme *c* binding motif. In fact, being covalently bond to the heme, Cys143 retains the His144 in its proximity yielding a 5cNO structure that is very similar to the 6cNO one.

Thus, based on the RR and MD data, it is tempting to speculate that the change of the redox state coupled to heme spin state/coordination alteration could be the putative signal transduction mechanism in the *Gs* sensors. An intriguing possibility in this line of thought is presented by the 6cHis−Met/5cHis equilibrium, which relies on the breaking of Fe−Met60 bond. Our results show that both proteins are stable in the two states and that changes due to Met coordination are significant and may extend beyond the H1−H2 loop toward the helices. As in most heme proteins, the axial methionine binds strongly to the ferrous state and can be detached only in the ferric state, as confirmed by our RR data. Therefore the following mechanism can be envisaged: the protein is kept blocked in the inactive/ferrous state, until a change in the environment redox potential oxidizes the protein, which releases Met60 and allows activation. This hypothesis reinforced by previously observed differences in redox potentials of 582 and 935 and present results, will be addresses in our future work.

Acknowledgment. This work was supported by Project Grants PTDC/BIA-PRO/74498/2006 to C.A.S. and PTDC/QUI/64550/2006 to S.T. from Fundação para a Ciência e a Tecnologia (FCT, Portugal); PICT07-01650 and UBA (08-X625) to M.A.M.; PICT06-25667 and PICT2006-459 to D.H.M.; U.S. Department of Energy's Office of Science, Biological and Environmental Research GTL Program under Contract No. DE-AC02-06CH11357. M.A.M. and D.M. are staff members of CONICET. M.P. and A.D.C are recipients of postdoctoral grants BPD/20571/2004 (FCT, Portugal) and CONICET, respectively. We thank M. Schiffer for critical reading of the manuscript and Y. Y. Londer for sensor plasmids and invaluable technical support.

References and Notes

(1) Rogers, K. R. Recent Advances in Biosensor Techniques for Environmental Monitoring. *Anal. Chim. Acta* **2006**, *568*, 222–231.

(2) Stock, A. M.; Robinson, V. L.; Goudreau, P. N. Two-Component Signal Transduction. *Annu. Rev. Biochem.* **2000**, *69*, 183–215.

(3) Chan, M. K. Recent Advances in Heme-Protein Sensors. *Curr. Opin. Chem. Biol.* **2001**, *5*, 216–222.

(4) Szurmant, H.; Ordal, G. W. Diversity in Chemotaxis Mechanisms among the Bacteria and Archaea. *Microbiol. Mol. Biol. Rev.* **2004**, *68*, 301–319.

(5) Wadhams, G. H.; Armitage, J. P. Making Sense of It All: Bacterial Chemotaxis. *Nat. Rev. Mol. Cell. Biol.* **2004**, *5*, 1024–1037.

(6) Fu, R.; Wall, J. D.; Voordouw, G. DcrA, a *c*-Type Heme-Containing Methyl-Accepting Protein from *Desulfovibrio vulgaris* Hildenborough, Senses the Oxygen Concentration or Redox Potential of the Environment. *J. Bacteriol.* **1994**, *176*, 344–350.

(7) Hao, B.; Isaza, C.; Arndt, J.; Soltis, M.; Chan, M. K. Structure-Based Mechanism of O_2 Sensing and Ligand Discrimination by the FixL Heme Domain of *Bradyrhizobium japonicum*. *Biochemistry* **2002**, *41*, 12952–12958.

(8) Yoshioka, S.; Kobayashi, K.; Yoshimura, H.; Uchida, T.; Kitagawa, T.; Aono, S. Biophysical Properties of a *c*-Type Heme in Chemotaxis Signal Transducer Protein DcrA. *Biochemistry* **2005**, *44*, 15406–15413.

(9) Londer, Y. Y.; Dementieva, I. S.; D'Ausilio, C. A.; Pokkuluri, P. R.; Schiffer, M. Characterization of a *c*-Type Heme-containing PAS Sensor Domain from *Geobacter sulfurreducens* Representing a Novel Family of Periplasmic Sensors in *Geobacteraceae* and Other Bacteria. *FEMS Microbiol. Lett.* **2006**, *258*, 173–181.

(10) Pokkuluri, P. R.; Pessanha, M.; Londer, Y. Y.; Wood, S. J.; Duke, N. E. C.; Wilton, R.; Catarino, T.; Salgueiro, C. A.; Schiffer, M. Structures and Solution Properties of Two Novel Periplasmic Sensor Domains with *c*-Type Heme from Chemotaxis Proteins of *Geobacter sulfurreducens*: Implications for Signal Transduction. *J. Mol. Biol.* **2008**, *377*, 1498–1517.

(11) Antonini, E.; Brunori, M. *Hemoglobin and Myoglobin in Their Reactions with Ligands*; North-Holland Publishing Co: Amsterdam, 1971.

(12) Hornak, V.; Abel, R.; Okur, A.; Strockbine, B.; Roitberg, A.; Simmerling, C. Comparison of Multiple Amber Force Fields and Development of Improved Protein Backbone Parameters. *Proteins. Struct., Funct. Genet.* **2006**, *65*, 712–725.

(13) Bikiel, D. E.; Boechi, L.; Capece, L.; Crespo, A.; De Biase, P. M.; Di Lella, S.; Gonzalez Lebrero, M. C.; Marti, M. A.; Nadra, A. D.; Perissinotti, L. L.; Scherlis, D. A.; Estrin, D. A. Modeling Heme Proteins Using Atomistic Simulations. *Phys. Chem. Chem. Phys.* **2006**, *8*, 5611–5628.

(14) Capece, L.; Estrin, D. A.; Marti, M. A. Dynamical Characterization of the Heme NO Oxygen Binding (HNOX) Domain. Insight into Soluble Guanylate Cyclase Allosteric Transition. *Biochemistry* **2008**, *47*, 9416–9427.

(15) De Biase, P. M.; Paggi, D. A.; Doctorovich, F.; Hildebrandt, P.; Estrin, D. A.; Murgida, D. H.; Marti, M. A. Molecular Basis for the Electric Field Modulation of Cytochrome *c* Structure and Function. *J. Am. Chem. Soc.* **2009**, *131*, 16248–16256.

(16) Marti, M. A.; Crespo, A.; Capece, L.; Boechi, L.; Bikiel, D. E.; Scherlis, D. A.; Estrin, D. A. Dioxygen Affinity in Heme Proteins Investigated Bycomputer Simulation. *J. Inorg. Biochem.* **2006**, *100*, 761–770.

(17) Crespo, A.; Scherlis, D. A.; Marti, M. A.; Ordejón, P.; Roitberg, A. E.; Estrin, D. A. A DFT-Based QM-MM Approach Designed for the Treatment of Large Molecular Systems: Application to Chorismate Mutase. *J. Phys. Chem. B* **2003**, *107*, 13728–13736.

(18) Siebert, F.; Hildebrandt, P. *Vibrational Spectroscopy in Life Science*: Wiley-VCH Verlag GmbH and Co., KGaA: Weinheim, 2008.

(19) Ioanoviciu, A.; Yukl, E. T.; Moenne-Loccoz, P.; de Montellano, P. R. Devs, a Heme-Containing Two-Component Oxygen Sensor of *Mycobacterium tuberculosis*. *Biochemistry* **2007**, *46*, 4250–4260.

(20) Inagaki, S.; Masuda, C.; Akaishi, T.; Nakajima, H.; Yoshioka, S.; Ohta, T.; Pal, B.; Kitagawa, T.; Aono, S. Spectroscopic and Redox Properties of a CooA Homologue from *Carboxydothermus hydrogenoformans*. *J. Biol. Chem.* **2005**, *280*, 3269–3274.

(21) Karow, D. S.; Pan, D.; Davis, J. H.; Behrends, S.; Mathies, R. A.; Marletta, M. A. Characterization of Functional Heme Domains from Soluble Guanylate Cyclase. *Biochemistry* **2005**, *44*, 16266–16274.

(22) Reynolds, M. F.; Parks, R. B.; Burstyn, J. N.; Shelver, D.; Thorsteinsson, M. V.; Kerby, R. L.; Roberts, G. P.; Vogel, K. M.; Spiro, T. G. Electronic Absorption, EPR, and Resonance Raman Spectroscopy of CooA, a CO-Sensing Transcription Activator from *R. rubrum*, Reveals a Five-Coordinate NO-Heme. *Biochemistry* **2000**, *39*, 388–396.

(23) Vogel, K. M.; Hu, S.; Spiro, T. G.; Dierks, E. A.; Yu, A. E.; Burstyn, J. N. Variable Forms of Soluble Guanylyl Cyclase: Protein-Ligand Interactions and the Issue of Activation by Carbon Monoxide. *J. Biol. Inorg. Chem.* **1999**, *4*, 804–813.

(24) Andrew, C. R.; Green, E. L.; Lawson, D. M.; Eady, R. R. Resonance Raman Studies of Cytochrome *c′* Support the Binding of NO and CO to Opposite Sides of the Heme: Implications for Ligand Discrimination in Heme-Based Sensors. *Biochemistry* **2001**, *40*, 4115–4122.

(25) Boon, E. M.; Davis, J. H.; Tran, R.; Karow, D. S.; Huang, S. H.; Pan, D.; Miazgowicz, M. M.; Mathies, R. A.; Marletta, M. A. Nitric Oxide Binding to Prokaryotic Homologs of the Soluble Guanylate Cyclase B1 H-NOX Domain. *J. Biol. Chem.* **2006**, *281*, 21892–21902.

(26) Andrew, C. R.; Kemper, L. J.; Busche, T. L.; Tiwari, A. M.; Kecskes, M. C.; Stafford, J. M.; Croft, L. C.; Lu, S.; Moenne-Loccoz, P.; Huston, W.; Moir, J. W.; Eady, R. R. Accessibility of the Distal Heme Face, Rather Than Fe-His Bond Strength, Determines the Heme-Nitrosyl Coordination Number of Cytochromes *c′*: Evidence from Spectroscopic Studies. *Biochemistry* **2005**, *44*, 8664–8672.

(27) Lukat-Rodgers, G. S.; Rodgers, K. R. Characterization of Ferrous FixL-Nitric Oxide Adducts by Resonance Raman Spectroscopy. *Biochemistry* **1997**, *36*, 4178–4187.

(28) Ford, P. C.; Fernandez, B. O.; Lim, M. D. Mechanism of Reductive Nitrosylation in Iron and Copper Models Relevant to Biological Systems. *Chem. Rev.* **2005**, *105*, 2439–2455.

(29) Ray, G. B.; Li, X. Y.; Ibers, J. A.; Sessler, J. L.; Spiro, T. G. How Far Can Proteins Bend the FeCO Unit? Distal Polar and Steric Effects in Heme Proteins and Models. *J. Am. Chem. Soc.* **1994**, *116*, 162–176.

(30) Martí, M. A.; Scherlis, D. A.; Doctorovich, F. A.; Ordejón, P. A.; Estrin, D. A. Modulation of NO Trans Effect in Heme Proteins: Implications in Guanylate Cyclase Activation. *J. Biol. Inorg. Chem.* **2003**, *8*, 595–600.

(31) Marti, M. A.; Capece, L.; Crespo, A.; Doctorovich, F.; Estrin, D. A. Nitric Oxide Interaction with Cytochrome *c′* and Its Relevance to Guanylate Cyclase. Why Does the Iron Histidine Bond Break. *J. Am. Chem. Soc.* **2005**, *127*, 7721–7728.

(32) Marti, M. A.; González Lebrero, M. C.; Roitberg, A. E.; Estrin, D. A. Bond or Cage Effect: How Nitrophorins Transport and Release Nitric Oxide. *J. Am. Chem. Soc.* **2008**, *130*, 1611–1618.

(33) Swails, J. M.; Meng, Y.; Walker, F. A.; Marti, M. A.; Estrin, D. A.; Roitberg, A. E. pH-Dependent Mechanism of Nitric Oxide Release in Nitrophorins 2 and 4. *J. Phys. Chem. B* **2009**, *113*, 1192–1201.

(34) Cooper, C. E. Nitric oxide and iron proteins. *Biochim. Biophys. Acta* **1999**, *1411*, 290–309.

(35) Viola, F.; Aime, S.; Coletta, M.; Desideri, A.; Fasano, M.; Paletti, S.; Tarricone, C.; Ascenzi, P. Azide, cyanide, fluoride, imidazole and pyridine binding to ferric and ferrous native horse heart cytochrome *c* and to its carboxymethylated derivative: a comparative study. *J. Inorg. Biochem.* **1996**, *62*, 213–222.

(36) Jones, M. G.; Bickar, D.; Wilson, M. T.; Brunori, M.; Colosimo, A.; Sarti, P. A re-examination of the reactions of cyanide with cytochrome *c* oxidase. *Biochem. J.* **1984**, *220*, 57–66.

(37) Stone, J. R.; Marletta, M. A. The ferrous heme of soluble guanylate cyclase: formation of hexacoordinate complexes with carbon monoxide and nitrosomethane. *Biochemistry* **1995**, *34*, 16397–16403.

(38) Mayburd, A. L.; Kassner, R. J. Mechanism and biological role of nitric oxide binding to cytochrome *c′*. *Biochemistry* **2002**, *41*, 11582–11591.

(39) Kassner, R. J. Ligand binding properties of cytochromes *c′*. *Biochim. Biophys. Acta* **1991**, *1058*, 8–12.

JP1029882